

International Conference on Space Optics—ICSO 2014

La Caleta, Tenerife, Canary Islands

7–10 October 2014

Edited by Zoran Sodnik, Bruno Cugny, and Nikos Karafolas



Earthcare MSI TIR detector qualification

L. Gomez Rojas

M. Chang

J. Everett

T. Phillips

et al.



International Conference on Space Optics — ICSO 2014, edited by Zoran Sodnik, Nikos Karafolas,
Bruno Cugny, Proc. of SPIE Vol. 10563, 105632D · © 2014 ESA and CNES
CCC code: 0277-786X/17/\$18 · doi: 10.1117/12.2304271

EARTHCARE MSI TIR DETECTOR QUALIFICATION

L. Gomez Rojas¹, M. Chang¹, J. Everett¹, T. Phillips¹, M. Sauer², K-W. Kruse², N. Nelms³,
A. Pérez Albiñana³, A. Crastes⁴

¹Surrey Satellite Technology Ltd., Guildford, UK, ²Astrium GmbH, Friedrichshafen, Germany,
³European Space Agency, Noordwijk, The Netherlands, ⁴Ulis-IR, Grenoble, France

Abstract -The ESA EarthCARE satellite mission objective is the observation of clouds and aerosols from low Earth orbit. The key spatial context providing instrument within the payload suite of 4 instruments is the Multi-Spectral Imager (MSI). This paper discusses the test program developed and implemented at SSTL for the formal qualification of the COTS micro-bolometer detectors for the TIR camera of the MSI. The comprehensive test campaign for the qualification of the detectors covered full electro-optical characterisation, life tests, environmental testing (thermal and mechanical), Particle Impact Noise Detection (PIND) tests, destructive physical analysis (DPA) and radiation tolerance assessment. Testing was undertaken at the specialist detector test facilities at SSTL. External facilities were called on for aspects of the programme. We describe the micro-bolometer arrays tested, the test benches developed for the program, test facilities, the test procedures and a summary of the test results. The qualification programme was completed in May 2014

I. INTRODUCTION

This paper discusses the tests performed at SSTL for the formal qualification of the single batch of UL03041 LWIR (uncooled micro-bolometers) detectors supplied by ULIS-IR for the TIR camera of the MSI on the EarthCARE mission [1]. The MSI is intended to provide information on the horizontal variability of the atmospheric conditions and to identify e.g. cloud type, textures, and temperature providing images in seven spectral bands, ranging from visible through short-wave infrared (VNS) to thermal infrared (TIR). It will provide spatial resolution at a ground sample distance of 500m, over a swath 150km wide.

The TIR camera consists of a single microbolometer area array detector of 384 x 288 pixels on a 35 μ m pitch placed within a two-stage imaging system. Microbolometers are highly reliable, small size, low input power, adapted to uncooled thermal imaging and have attracted interest for space applications in recent years [2],[3],[4]. Here we present the full qualification programme for their use in the EarthCARE mission. Production lot testing and environmental testing on representative samples was performed by Ulis and is not covered in this paper. Subsequent acceptance and qualification testing made use of facilities setup at SSTL (described in the relevant section of this paper), as well as existing facilities at Spur Electronics, API Technologies, ESTEC and Université Catholique of Louvain (UCL). The testing at Spur was concerned primarily with measuring the physical characteristics of the devices; seal, PIND and physical destructive analysis (DPA). Thermal cycling tests were performed at API technologies and irradiation tests performed at both ESTEC Co60 facility and UCL HIF facility

II. DEVICES TESTED

The microbolometers to be used in the EarthCARE MSI are 384 x 288 pixel devices with a pixel pitch of 35 μ m (Fig. 1). The detector element is a film of amorphous silicon suspended on thin legs (for thermal isolation) above a CMOS ROIC [5]. The devices are operated in 'rolling blind' mode, with a pulsed voltage bias (shown as VFID in Fig 1) being applied one line at a time. During this time the resultant current through the microbolometer is integrated on a CMOS CTIA Capacitance Trans Impedance Amplifier (with fixed capacitance) so that the change in resistance (due to the change in temperature caused by IR absorption in the amorphous silicon film) can be measured. The device also has good linearity. The use of an on-chip CTIA stage gives a linearity error of less than 1%. The device has a thermoelectric cooler for stabilization of the device temperature, which is normally in the range 25°C-30°C for best performance.

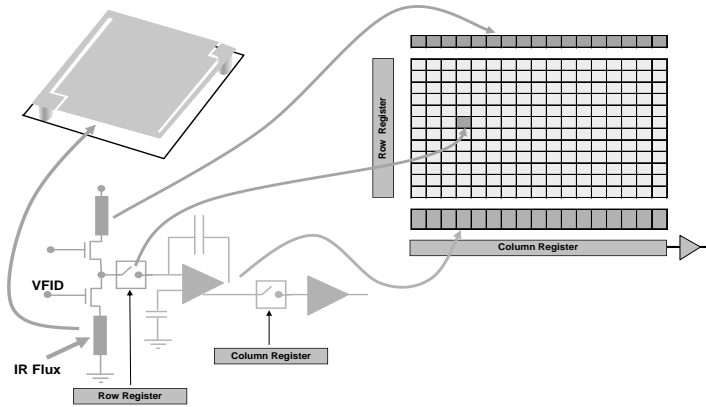


Fig 1. Schematic of a UL 03041 pixel Ulis microbolometer array

A. Operating Conditions

During the mission the detector will be used in TDI (Time Delay Integration) mode. The detector will be read out in 5 blocks of 20 rows each, with TDI applied to each odd numbered block such that blocks 1, 3 and 5 represent the optical scene bands from the dichroic filters; band 7 ($\lambda_{\text{centre}} = 8.8\mu\text{m}$, $\text{BW} = 0.9\mu\text{m}$), band 8 ($\lambda_{\text{centre}} = 10.8\mu\text{m}$, $\text{BW} = 0.9\mu\text{m}$) and band 9 ($\lambda_{\text{centre}} = 12\mu\text{m}$, $\text{BW} = 0.9\mu\text{m}$) of the MSI TIR. The TDI processing is performed in the front end electronics (FEE) by adding the first line of a block for the first ground line interval to the second line of the block during the second ground line interval etc. to the 20th line (i.e. In TDI mode signals from N rows in each image area are co-added from N successive frames). During each ground line interval the detector is readout multiple times (nominally 5) and the pixel data added to get the data for a ground line interval ready for TDI addition.

III. QUALIFICATION TESTING

From the original batch received at SSTL, 11 micro-bolometers underwent the tests shown in the flow diagram depicted in Fig 2. For all tests adequate ESD protection (e.g. wearing a wrist strap) where applicable was used.

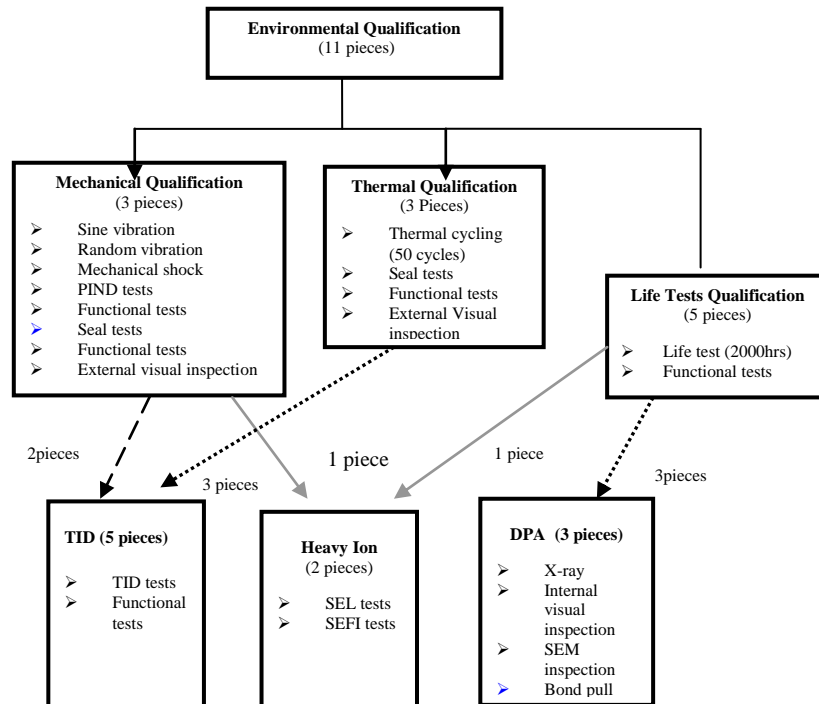


Fig 2. Flow diagram of qualification test campaign for the UL 03041

A. Functional tests

For all environmental tests apart from those of a destructive nature all devices were functionally tested before and after the specific environmental test sequence. The devices subjected to particularly long tests were functionally tested at intermediate steps to ensure the integrity of the devices or determine premature failure.

B. SSTL's electro-optical test facility.

The general schematic diagram for the tests setup is shown in Fig 3. The detector was mounted in a dedicated 'flex' board (with sprung loaded sockets to avoid soldering of the detectors and allow easy mounting) connected to the FEE board. The flex board was mounted on a specifically designed jig with pipe connections for temperature control. Heat was removed from the hot side of the detector by a re-circulated liquid coolant.

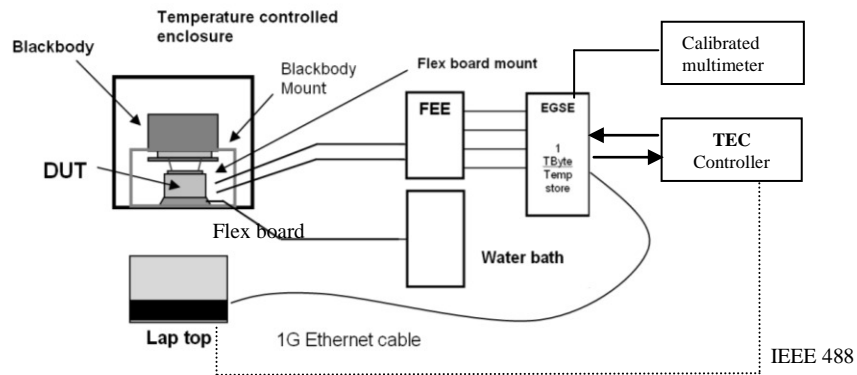


Fig. 3: Schematic diagram of microbolometer test set up

The detector clocks and biases were supplied by the FEE board powered by the Electrical Ground Support Equipment (EGSE) board programmed from the host PC via a 1G Ethernet interface. The optical stimulation was provided by a wide area black body mounted inside the temperature enclosure (see Fig. 3) to allow for an f/1 signal to the system. The accuracy of the measurement system depends on the resolution of the black body control unit, water bath and front end electronics hence minor changes on the test conditions were expected during the measurements.

IV. MECHANICAL QUALIFICATION

A. Vibration Testing

A dedicated test cube with tapped holes on the sides and top was used for these tests. The cube was bolted onto an intermediate plate which bolts directly onto the shaker. The cube allowed for testing all axes without the need for a slip table. The detector was bolted directly onto the cube where a facet had been modified to accommodate the detector ensuring that the device plus pins sat flat on the surface of the cube keeping all pins connected to ground by means of a nylon clamp fixed onto the cube.

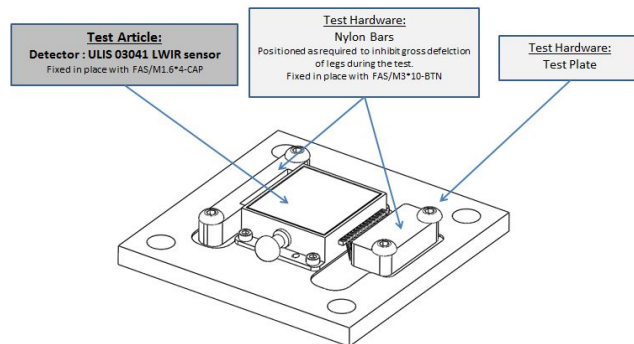
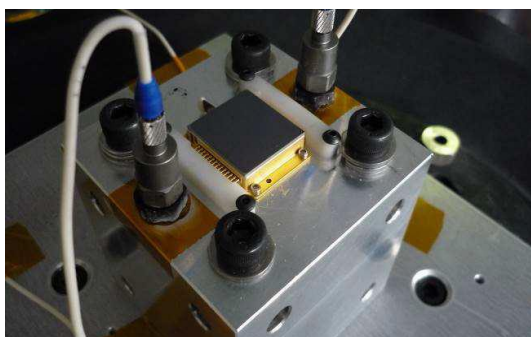


Fig. 4 Detector test mount with ULIS 03041 device mounted on (left) , test mount (right)

The test article was required to be tested in all three axes. The order of testing in each axis was as follows:

Low Level Sine

A low level instrumentation check was carried out for each axis to ensure that the test setup is functioning correctly,

Qualification Random

Random vibration levels were derived from the tests results of the MSI structural model vibration campaign. An accelerometer was placed at the location of the chip and the levels during the test measured. The output spectrum was then enveloped to produce a test profile used during vibration

Qualification Sine

The qualification levels for combined sine and quasi-static are shown in Table 1

Table 1: Combined sine and quasi-static qualification levels (all axes)

Axis	Frequency [Hz]	Qualification
Out of plane (X)	5 - 24	11.0 mm
	24 -100	24 g
In Plane (Y & Z)	5-20	10.0 mm
	20-100	16 g
Sweep Rate		2 Oct/min
		1 sweep-up

Functional Test Results

Table 2 shows a summary of the change in electro-optical parameters after vibration

Table 2: Summary of functionality results after vibration testing

Device #	Power supply currents changed during test	No of Defect pixels changed during test	Δ TEC current @ 30°C %	Δ NEDT %	Δ Responsivity @ 30°C %	Comments (pass/fail)
SN 09042	V skimming	0	1.412	0.123	-2.092	Pass
SN 09044	V skimming	0	0.969	0.692	-0.104	Pass
SN 11026	V skimming	0	2.728	-1.304	-2.226	Pass

B. Shock Testing

Same test cube used during the vibration campaign was used for these tests. The cube allowed for measuring on all axes simultaneously. The detector was bolted onto the side of the cube ensuring that the device plus pins sat flat on the surface and all pins were connected to ground. The pins were held in position by means of a nylon clamp fixed onto the plate. The Test Levels for the detector shock qualification testing were derived from the shock measurements performed on the Engineering Confidence Model [ECM] of the MSI. Table 3 shows a summary of the change in electro-optical parameters after shock testing

Table 3: Summary of functionality results after shock testing

Device #	Power supply currents changed during test	No of Defect pixels changed during test	Δ TEC current @ 30°C %	Δ NEDT %	Δ Responsivity 30°C %	Comments (pass/fail)
SN 09042	V skimming	0	-0.689	-0.570	-2.004	Pass
SN 09044	V skimming	0	-2.132	0.313	-0.312	Pass
SN 11026	V skimming	0	-0.204	-1.276	0.484	Pass

V. THERMAL QUALIFICATION

Thermal cycling was carried out at API Technologies in an automated thermal vacuum chamber following MIL STD 883 Method 1010 condition A which specifies a transfer time <1min and dwell time of 10 min with a maximum and minimum temperatures of +85⁰C and -55⁰C respectively. The automated chamber provided a transfer time of 10s with a maximum and minimum temperatures of +89⁰C and -58⁰C within the specification of the MIL STD. The detectors were placed inside the chamber and cycled 50 times. Table 4 shows a summary of the change in electro-optical parameters after thermal cycling

Table 4: Summary of functionality results after Thermal cycling

Device #	Power supply currents changed during test	No of Defect pixels changed during test	Δ TEC current @ 30°C %	Δ NEDT %	Δ Responsivity @ 30°C %	Comments (pass/fail)
SN 11022	V skimming, V bus	0	11.99468	-1405.28	93.26229	FAIL
SN 09037	V skimming, V bus	0	-2.62391	1.39801	-3.62178	Pass
SN 09047	V skimming, V bus	0	-2.46499	2.375722	0.664688	Pass

Note device 11022 suffered major loss in responsivity after seal failure during environmental testing but it was demonstrated that it can be fully recovered in flight. Furthermore, the sampling number for such a test is not significant when it comes to extrapolating a failure probability. Ulis has provided additional information regarding this MIL STD 883 M 1010 thermal qualification test for 50 cycles : the failure rate tested on 57 detectors shows a reliability rate of 99.99% with a confidence level of 60% and for 400 cycles it can go down to 99.78% with the same confidence level

VI. LIFE TESTS

Life tests were carried out on a dedicated MSI FEE Breadboard that can clock 5 devices simultaneously. The tests were performed on TDI mode. The 5 components were operated for a total of 1222 hours at the maximum rated temperature of 65°C. The devices were taken out after 168 and 504 hours and tested for functionality Table 5 shows a summary of the change in electro-optical parameters after 1222 hours

Table 5: Summary of functionality results after 1222 hours of life testing

Device #	Power supply currents changed during test	No of Defect pixels changed during test	Δ TEC current @ 30°C %	Δ NEDT %	Δ Responsivity @ 30°C %	Comments (pass/fail)
SN 09027	V skimming, V bus, Vdda	0	-3.478	-0.301	1.764	Pass
SN 10025	V skimming, V bus, Vddl	0	-4.985	-1.583	4.414	Pass
SN 10024	V skimming, V dda, Vddl	0	-6.793	0.062	1.065	Pass
SN 09041	V skimming, V bus, Vdda, Vddl	0	-0.916	2.455	0.430	Pass
SN 09024	V skimming, V bus, Vdda	0	9.228	0.761	1.192	Pass

VII. PIND and DPA

All the devices from the mechanical test batch were subjected to a PIND test to verify that no parts inside the package became loose after the mechanical tests (vibration and shock). All parts passed. The devices were then subjected to physical destructive analysis. The tests were performed by Spur electronics and the results are reported on a confidential document not referenced in this paper

VIII. RADIATION TESTING

A. Total Ionizing Dose

Cobalt60 irradiations were carried out during June 25-26 2013 at the irradiation facility at ESTEC. Two devices were irradiated biased (#10024 and #09047) and two irradiated unbiased (#09024 and #10025). All devices were irradiated up to 10krad(Si). The devices were measured before and after the irradiations and for the biased devices the bias currents monitored during the exposure. A monitor device (#09037) was also measured before and after the irradiations. Functionality post rad tests were started immediately on return to SSTL, followed by annealing tests after 1 week storage at RT (Room temperature) and after 168 hours at 100°C. Fig. 5 shows a photograph of the irradiation set up

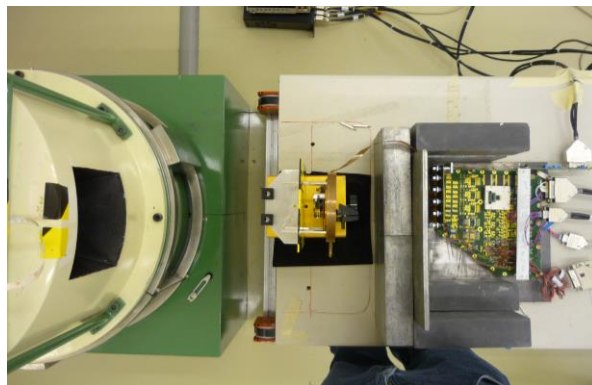


Fig. 5. Irradiation setup showing the lead blocks used for shielding the drive electronics

Table 6 summarises the post-irradiation performance showing the bias currents that changed during Co60 irradiation and the change in percentage of the electro-optical parameters. All parameters were also measured after 24hrs, 1 week anneal at RT and 100°C showing a small change of less than 5% from the values shown

Table 6 Percentage of change of electro-optical parameters after Co60 irradiation

Device #	Power supply currents changed during test	Δ TEC current @ 27°C	Δ NEDT	Δ Responsivity @ 27°C
SN 09024	V skimming, Vddl	2.371	4.951	-1.679
SN 09047	V skimming, Vddl	1.611	6.425	1.425
SN 10024	None	2.570	1.783	0.542
SN 10025	V skimming, Vddl	5.211	19.572	-2.297
SN 09037	V skimming, V bus, Vddl	3.790	7.891	0.454

B. Heavy Ion Testing

Heavy Ion tests were performed on 18 November 2013 at the heavy ion facility (HIF) at the Université Catholique de Louvain (UCL), Louvain la Neuve, Belgium. This facility gives a beam homogeneous to $\pm 10\%$ over a 25 mm diameter. Ion cocktail number 1 (High LET, M/Q = 5) was used (Xe, Kr Ar and Ne ions). For these tests only Kr and Ar ions were used giving a maximum of 40.4 MeV/mg/cm² at normal incidence.

Two devices were irradiated and a total of 5 hours beam time was used for these tests. The ion flux at the device was adjusted between 2000 and 12000 ions/cm²/s. Power supply currents to the device were monitored using a *tcl* program that scanned the outputs of two digital voltmeters. Each supply had a current limit which, if exceeded (due to a latch-up event), triggered an event flag and automatic power off. Following such event the device had to manually be turned on and the monitoring software re-initiated. During exposure all bias currents were monitored for SELs and multiple images taken to analyse for image quality and potential degradation due to overheating a line of microbolometers. Figure 6 shows photographs of the test board inside the vacuum chamber

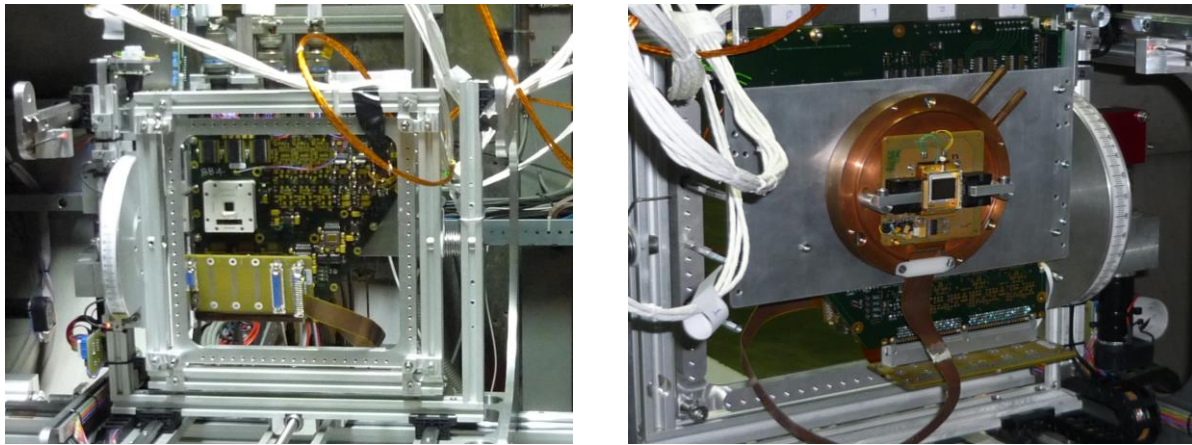


Fig. 6. Photographs of the test board inside the HIF chamber. Drive electronics positioned behind the DUT (left). The device at normal incidence to the beam (right)

The devices were tested at 3 different energies as shown in Table 7. During exposure all bias currents were monitored for SELs and SEUs and multiple images taken to analyse for SEFIs or any other effects that could occur. Due to mechanical constraints both devices could not be tested at the same LET values; a higher than 42 degrees and 40 degrees for devices 10016 and 11022 of tilt was not practicably achieved, hence maximum LET values of 20.76 and 21.4 MeV/mg/cm² were used during the tests. Table 7 summarizes the irradiations

Table 7 Summary of Heavy Ion irradiation

Device #	LETs (MeV/mg/cm ²)	Flux (ions/ cm ² /s)	Fluence (ions/ cm ²)	Facility
SN 10016	40.4, 21.4, 15.9	2000 -12000	1E7	HIF
SN 11022	40.4, 20.76, 15.9	2000 - 12000	1E7	HIF

Fig. 7 shows the SEL cross section measured and the weibull fit for the raw data for both devices irradiated. Both devices showed a very similar behaviour with latch ups down to 15.9 MeV/mg/cm².

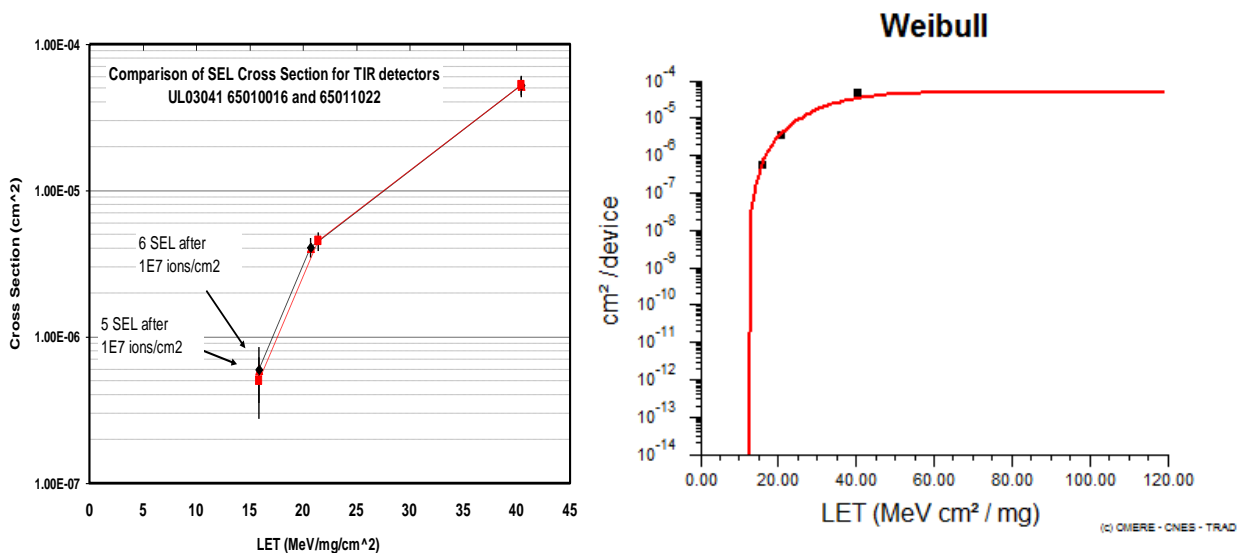


Fig. 7. Measured cross section for SEL events for devices 10016 and 11022. Error bars are 1σ (left) and weibull fit of raw data (right)

Due to practical issues a higher than 40 degrees of tilt was not practicably achieved hence LET values of greater than 9 MeV/mg/cm² were not feasible using lower LET ions so given the low SEL count the minimum LET the

devices were tested at was 15.9 MeV/mg/cm². The SEL rate and threshold estimated using OMERE analysis software. Table 8 shows mission daily SEL rate predictions for nominal background and solar flare conditions.

Table 8 SEL rate predictions for both UL03041 devices tested

	<u>UL03041 (65010016)</u>	<u>UL03041 (65011022)</u>
Nominal (/day)	8.47E-06	9.11E-06
Solar Flare (worst day) (/day)	1.69E-03	1.81E-03
Solar flare (Peak 5 min rate) (/day)	6.16E-03	6.62E-03
Total Mission Rate (with peak 5 min flare rate) *	2.77E-02	2.98E-02

(*Assuming 1 large anomalous solar flare lasting 3 days)

The rates were calculated using the cross section plots provided in Figure 7 and OMERE analysis software. The Weibull parameters used were: W=25, S=2.4 and the saturated cross-section was taken at the 40MeV test point.

Table 9 summarises the SEUs measured for both devices at all the LETs tested. Any event during beam exposure that did not trigger an automatic power off but corrupted the image capture was recorded. The images were taken at a rate of approximately 1 in 13 ms and analysed back at SSTL. The images were analysed using Image J and the data correlated to the latch up log files created during the exposure at each run.

Table 9 Number of SEUs measured for each of the two detectors tested at different LET values

Device LET (MeV/mg/cm ²)	65010016 # of events	65011022 # of events
15.9	2	3
20.76		3
21.4	3	
40.4	2	2

IX. CONCLUSIONS

Out of all the detectors tested only one suffered major loss in responsivity after seal failure during environmental testing but it was demonstrated that it can be fully recovered in flight. All the remaining detectors performed well and any small changes measured during the whole campaign do not have a meaningful impact on the mission. It was also demonstrated that most of the changes, in any of the parameters measured, were not due to a degradation caused by the tests, but by minor changes on the test conditions experienced during testing, Vskimming being the most affected. However this bias is not relevant in the electro-optical performance of the detector. Furthermore, these small changes will not have an effect during the mission as the device gets calibrated every orbit. The detectors also showed excellent radiation hardness for both total dose and Single event effects to the levels required by the programme. Hence it can be concluded that the arrays tested are suitable for use on the EarthCARE mission.

X. REFERENCES

- [1] Bézy, J.-L., Ingmann, P., Leibrandt, W., Lin, C.-C., Meynart, R. and Silvestrin, P., "System, spacecraft, and instrument concepts for the ESA Earth Explorer EarthCARE Mission", Proc SPIE, 5978, 59780J (2005).
- [2] J. Johnson, J. Shaw, R. Lawrence, P.Nugent, L.Dobeck, L.Spangler, "Long-wave infrared imaging of vegetation for detecting leaking CO2 gas", Journal of applied Remote Sensing, pp 063612, Vol. 6, 2012
- [3] L. Phong and T. Pope, "Linear Arrays of Microbolometers for Space Applications" IEEE Sensors Conference, 2008, 26-29 Oct 2008, pp 1344-1347
- [4] G. Hopkinson, R. Harboe-Sorensen, B. Leone, R. Meynart, A. Mohammadzadeh, W.Rabaud "Radiation Effects in InGaAs and Microbolometer Infrared Sensor Arrays for Space Applications, IEEE Transactions on Nuclear Science, Vol. 55, No. 6, Dec 2008.
- [5] Mottin, E., Bain, A., Martin, J. L., Ouvrier-Buffet, J. L., Bisotto, S., Yon, J. J., and Tissot, J. L., "Uncooled amorphous silicon technology enhancement for 25µm pixel pitch achievement", Proc SPIE, 4820, 200 (2003)